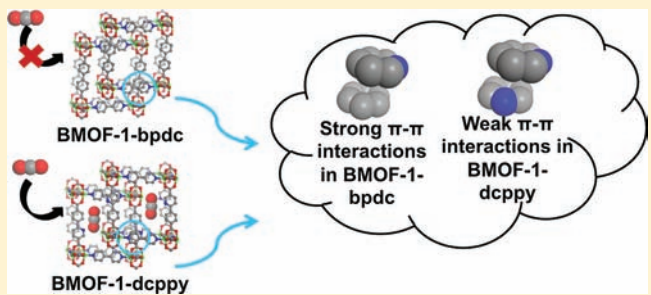# Single-Atom Ligand Changes Affect Breathing in an Extended Metal−Organic Framework

Phuong V. Dau, Min Kim, Sergio J. Garibay, Frédéric H. L. Münch, Curtis E. Moore, and Seth M. Cohen*

Department of Chemistry and Biochemistry, University of California, San Diego, La Jolla, California 92093, United States

Ⓢ *Supporting Information*

ABSTRACT: 2-Phenylpyridine-5,4′-dicarboxylic acid (**1**, dcppy), a derivative of 4,4′-biphenyldicarboxylic (**2**, bpdc) was used as the organic linking component for several metal–organic frameworks (MOFs). The pyridine component of **1** does not interfere with the solvothermal synthetic procedure, and hence both **1** and **2** form similar isoreticular MOFs. Zr^{4+}-based UiO-67-dcppy, Al^{3+}-based DUT-5-dcppy, Zn^{2+}-based DMOF-1-dcppy, and interpenetrated Zn^{2+}-based BMOF-1-dcppy were readily synthesized from **1**. Similarly, isostructural frameworks from **2** were prepared (UiO-67, DUT-5, DMOF-1-bpdc, and interpenetrated BMOF-1-bpdc). The structures and physical properties of these frameworks were characterized by powder X-ray diffraction (PXRD), single X-ray diffraction (XRD), thermogravimetric analysis (TGA), and gas sorption analysis. Generally, frameworks prepared from **1** or **2** displayed similar properties; however, gas sorption data showed that BMOF-1-dcppy displayed a very large hysteresis with N_2 and CO_2 suggestive of possible framework flexibility. In contrast, the analogous framework prepared from **2** (BMOF-1-bpdc) showed low uptake of N_2 and CO_2. The substantial difference in the gas sorption behavior of these MOFs is attributed to the pyridine nature of **1** that results in weakened $\pi-\pi$ interactions between the interpenetrated nets.

INTRODUCTION

Metal−organic frameworks (MOFs) with structurally well-defined nanoscale channels are of great interest for their use in gas storage,[1] separations,[2] catalysis,[3] and other technologies.[4] Numerous types of MOFs have been constructed with varying choices of metal ions and organic bridging ligands to afford materials with tailored channels and cavities. Kitagawa and co-workers have categorized MOFs into first, second, and third generation materials.[5] The first generation of MOFs are microporous frameworks that remain porous only with the inclusion of guest molecules and show irreversibly structural transformations after removal of guest molecules. The second generation of MOFs are stable and permanently porous frameworks, even when guest molecules are absent from the pores. Finally, the third generation of MOFs are flexible and dynamic frameworks, which respond to guest molecules, light, or other stimuli resulting in reversible structural transformations (i.e., responsive materials).[2] In comparison with rigid MOFs, the structure of flexible MOFs can be changed upon interaction with guest molecules. Factors such as the shape or size of the guest, or specific guest−surface interactions (e.g., hydrogen bonding) can induce a structural rearrangement in flexible MOFs. As a result, flexible MOFs can often show selective uptake of different guest molecules when compared to robust MOFs.[6,7] The selectivity and flexibility of MOFs can be modulated by modifications of the organic bridging ligands.[8−13]

In the construction of MOFs, multidentate aromatic ligands such as 1,4-benzene dicarboxylic acid, 1,3,5-benzenetricarbox-ylic acid, and 4,4′-bipyridine are typically used as the organic building blocks due to the their rigid structures.[14−17] Typically, the size and functionality of MOF pores can be tuned by modifying the organic ligand. Several MOFs have been extended in size and decorated with functional groups by simply utilizing longer or functionalized organic linkers.[18,19] Furthermore, physical properties of MOFs have been shown to be tunable by this approach. In particular, extended frameworks with surfaces bearing vacant or exposed metal centers are intriguing materials since these can greatly enhance the gas uptake or serve as a source for catalytic activity. Metal pyridine complexes such as $[Ru(bpy)_3]^{2+}$ (bpy = 2,2′-bipyridine) and $[Ir(ppy)_2(bpy)]^+$ (ppy = 2-phenylpyridine) and their derivatives[20] have a wide range of potential applications including water oxidation,[21] hydrogen production,[22,23] carbon dioxide reduction,[24] and C−H activation.[25] Thus, pyridine-contained ligands may be useful in the development of functional materials. Recently, 2,2′-bipyridine-5,5′-dicaboxylic acid (bpydc) was incorporated into an Al^{3+}-based framework (MOF-253), featuring open 2,2′-bipyridine ligand sites.[26] Subsequent complexation of Pd^{2+} and Cu^{2+} to the bpy linkers in MOF-253 was shown to enhance the selectivity for the adsorption of CO_2 over N_2. However, the use of $h_2$bpydc to make MOFs is limited to hard oxophilic cations to avoid competitive complexation by the chelating $h_2$bpydc ligand. As a

Scheme 1. Integration of 1 and 2 into Zr^{4+}, Al^{3+}, and Zn^{2+}-Based MOFs^a
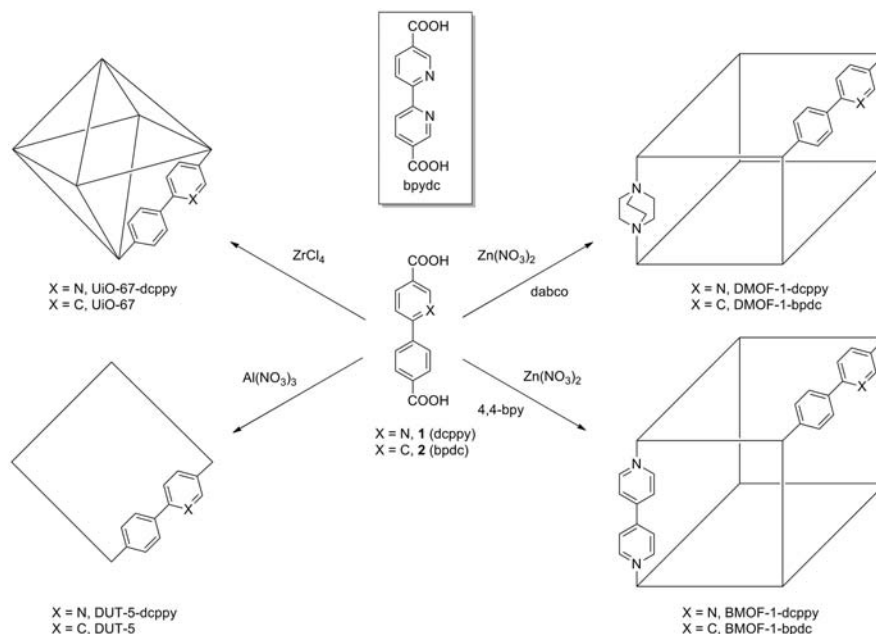
^{a}For comparison, the bpydc ligand is shown in the raised box.

consequence, it is expected that the bpydc ligand will be restricted with respect to the scope of MOF materials it can be used to prepare, while preserving the open bpy ligand site.

In light of this limitation, ligand **1** was designed as a more versatile alternative to bpydc. When compared with bpydc, the pyridine-phenyl core of **1** still possesses the ability to form a wide variety of complexes with metal ions. However, unlike bpydc, chelation by the pyridine-phenyl core of **1** requires C−H activation (i.e., cyclometalation), which is unlikely to occur with the high oxidation state metals ions used in the formation of MOFs. Thus, **1** should be compatible with a variety of different metal ions to form different types of MOFs. With these advantages in mind, **1** can provide a more diverse platform for creating exposed metal centers within MOFs. This approach was recently validated by the work of Lin and co-workers.[27] Complexes of **1** and Ir^{3+} ($[Ir^{3+}(1)(Cp*)(1)Cl]$ and $[Ir^{3+}(1)_2(H_2O)_2]^+$, where Cp* = pentamethylcyclopentadienyl), were doped into the UiO-67 frameworks and demonstrated catalytic activity including water oxidation, carbon dioxide reduction, and organic photocatalysis. It was found that the steric demand of the pre-cyclometalated "metalloligands" allowed for only fractional incorporation into the UiO-67 framework (a mixed-ligand framework was based with the metalloligands and **2**). Herein, we complement these existing studies, showing that **1** can be quantitatively introduced into a variety of MOF topologies. Additionally, in order to examine the effects of the pyridine group of **1** on the physical properties of these MOFs, isoreticular MOFs were synthesized from the simple biphenyl ligand **2** for comparison (Scheme 1).

■ EXPERIMENTAL METHODS

General. Starting materials and solvents were purchased and used without further purification from commercial suppliers (Sigma-Aldrich, Alfa Aesar, EMD, TCI, Cambridge Isotope Laboratories, Inc., and others). UiO-67 and DUT-5 were synthesized following reported procedures.[28,29]

Synthesis of UiO-67-dcppy. **1** (85 mg, 0.35 mmol) and $ZrCl_4$ (82 mg, 0.35 mmol) were dissolved in *N,N*-dimethylformamide

(DMF, 4 mL) in a Teflon-lined Parr stainless steel vessel (20 mL). The vessel was sealed and placed in a preheated oven at 120 °C for 24 h. After being cooled to room temperature, the reaction mixture was separated from the white crystalline powder by centrifugation and the remaining solid was washed with DMF (3 × 10 mL). The solvent was then exchanged for CH_2Cl_2 (3 × 10 mL) where the powder was left for 3 days, replacing the solution with fresh CH_2Cl_2 every 24 h.

Synthesis of DUT-5-dcppy. **1** (131 mg, 0.54 mmol) and $Al(NO_3)_3 \cdot 9H_2O$ (263 mg, 1.4 mmol) were dissolved in DMF (15 mL) in a Teflon-lined Parr stainless steel vessel (100 mL). The vessel was sealed and placed in a preheated isotherm oven at 120 °C for 24 h. After being cooled to room temperature, the reaction mixture was separated from the white crystalline powder by centrifugation and the remaining solid was washed with DMF (3 × 10 mL). The solvent was then exchanged for CH_2Cl_2 (3 × 10 mL) where the powder was left for 3 days, replacing the solution with fresh CH_2Cl_2 every 24 h.

Synthesis of DMOF-1-dcppy. **1** (97 mg, 0.4 mmol) and $Zn(NO_3)_2 \cdot 6H_2O$ (119 mg, 0.4 mmol) were dissolved in DMF (15 mL). To this solution, 1,4-diazabicyclo[2.2.2]octane (dabco, 68 mg, 0.6 mmol) was added, which formed a white precipitate that was removed by filtration through a fine glass frit. The solution was then transferred to a scintillation vial and heated at a rate of 2.5 °C/min from 35 to 100 °C. The temperature was then held for 24 h and then cooled to 35 °C at a rate of 2.5 °C/min. The resulting clear rectangular crystals were washed with DMF (3 × 10 mL). The solvent was then exchanged for ethyl acetate (3 × 10 mL), where the crystals were left for 3 days, replacing the solution with fresh ethyl acetate every 24 h.

Synthesis of DMOF-1-bpdc. **2** (49 mg, 0.2 mmol) and $Zn(NO_3)_2 \cdot 6H_2O$ (119 mg, 0.4 mmol) were dissolved in DMF (15 mL). To this solution, dabco (34 mg, 0.3 mmol) was added, which formed a white precipitate that was removed by filtration through a fine glass frit. The solution was then transferred to a scintillation vial and heated at a rate of 2.5 °C/min from 35 to 100 °C. The temperature was then held for 24 h and then cooled to 35 °C at a rate of 2.5 °C/min. The resulting clear rectangular crystals were washed with DMF (3 × 10 mL). The solvent was then exchanged for ethyl acetate (3 × 10 mL), where the crystals were left for 3 days, replacing the solution with fresh ethyl acetate every 24 h.

Synthesis of BMOF-1-dcppy. **1** (49 mg, 0.2 mmol) and $Zn(NO_3)_2 \cdot 6H_2O$ (119 mg, 0.4 mmol) were dissolved in DMF (15 mL). To this solution, 4,4′-bipyridine (4,4′-bpy, 32 mg, 0.2 mmol) was

added. The solution was then transferred to a scintillation vial and heated at a rate of 2.5 °C/min from 35 to 100 °C. The temperature was then held for 24 h and then cooled to 35 °C at a rate of 2.5 °C/min. The resulting clear rod-type crystals were then washed with DMF (3 × 10 mL). The solvent was then exchanged for ethyl acetate (3 × 10 mL) where the crystals were left for 3 days, replacing the solution with fresh ethyl acetate every 24 h.

Synthesis of BMOF-1-bpdc. 2 (49 mg, 0.2 mmol) and Zn(NO₃)₂·6H₂O (119 mg, 0.4 mmol) were dissolved in DMF (15 mL). To this solution, 4,4′-bpy (32 mg, 0.2 mmol) was added. The solution was then transferred to a scintillation vial and heated at a rate of 2.5 °C/min from 35 to 100 °C. The temperature was then held for 24 h and then cooled to 35 °C at a rate of 2.5 °C/min. The resulting clear rod-type crystals were then washed with DMF (3 × 10 mL). The solvent was then exchanged for ethyl acetate (3 × 10 mL) where the crystals were left for 3 days, replacing the solution with fresh ethyl acetate every 24 h.

Digestion and Analysis by ¹H NMR of UiO-67, UiO-67-dcppy, DUT-5, and DUT-5-dcppy. Approximately 10 mg of MOF material was dried under a vacuum at 100 °C overnight and digested with sonication in 580 μL of CD₃OD and 20 μL of HF (48% aqueous solution).

Digestion and Analysis by ¹H NMR of DMOF-1-bpdc, DMOF-1-dcppy, BMOF-1-bpdc, and BMOF-1-dcppy. Approximately 10 mg of the material was dried under a vacuum at 100 °C overnight and digested with sonication in 580 μL of DMSO-d₆ and 20 μL of DCl (35% aqueous solution).

Powder X-ray Diffraction. Prior to PXRD analysis, UiO-67, UiO-67-dcppy, DUT-5, and DUT-5-dcppy was dried at 100 °C for 1 h. DMOF-1-bpdc, DMOF-1-dcppy, BMOF-1-bpdc, and BMOF-1-dcppy were air-dried for 1 min prior to PXRD data collection. PXRD data were collected at ambient temperature on a Bruker D8 Advance diffractometer using a LynxEye detector at 40 kV, 40 mA for Cu Kα (λ = 1.5418 Å), with a scan speed of 1 s/step, a step size of 0.02° in 2θ, and a 2θ range of 4−45 °C.

BET Surface Area Analysis. For UiO-67, UiO-67-dcppy, DUT-5, and DUT-5-dcppy 30−100 mg of MOF was evacuated under vacuum for ~18 h at room temperature. For DMOF-1-dcppy, DMOF-1-bpdc, BMOF-1-dcppy, and BMOF-1-bpdc, 30−100 mg of MOF was evacuated under vacuum for only 2 min at room temperature, as these MOFs were found to be unstable under longer evacuation times. Samples were then transferred to a preweighed sample tube and degassed at 105 °C on a Micromeritics ASAP 2020 Adsorption Analyzer for a minimum of 12 h or until the outgas rate was <5 μmHg/min. The sample tube was reweighed to obtain a consistent mass for the degassed MOF. Brunauer−Emmett−Teller (BET) surface area (m²/g) measurements were collected at 77 K with N₂ on a Micromeritics ASAP 2020 Adsorption Analyzer using a volumetric technique. The sample was then manually degassed at 105 °C for minimum of 2 h before the CO₂ uptake measurement at 196 K.

Single Crystal X-ray Diffraction. Single crystals of DMOF-1-bpdc, DMOF-1-dcppy, and BMOF-1-dcppy taken from ethyl acetate were mounted on nylon loops with paratone oil and placed under a nitrogen cold stream (200 K). Because of the fragility of BMOF-1-bpdc, the single-crystal diffraction data was obtained at 260 K. Data were collected on a Bruker Apex diffractometer using Mo Kα (λ = 0.71073 Å) radiation controlled using the APEX 2010 software package. A semiempirical method utilizing equivalents was employed to correct for absorption. All data collections were solved and refined using the SHELXTL software suite.[30] All structures were treated with the "SQUEEZE" protocol in PLATON[31] to account for partially occupied or disordered solvent (e.g., DMF, EtOAc) within the porous frameworks. Structural details can be obtained from the Cambridge Crystallographic Data Centre (CCDC) under deposition numbers 857740, 857741, 857742, and 857743.

Thermal Analysis. Approximately 10−15 mg of MOF was used for thermogravimetric analysis (TGA) measurements, which were obtained immediately after collection of gas sorption data (i.e., activated samples). Samples were analyzed under a stream of N₂ (10 mL/min) using a TA Instrument Q600 SDT running from room temperature to 800 °C (for UiO and DUT-5 series) or to 600 °C (for DMOF and BMOF series) with a ramping rate of 5 °C/min.

■ RESULTS AND DISCUSSION

The Zr⁴⁺-based UiO-67 (UiO = University of Oslo) and Al³⁺-based DUT-5 (DUT = Dresden University of Technology) frameworks are known for their chemical stability.[28,29] UiO-67 is comprised of Zr₆O₄(OH)₄ secondary building units (SBUs) and 2. DUT-5 is made up of 2 and infinite SBUs, in which each Al³⁺ ion is six-coordinate in a distorted octahedral symmetry. The axial positions of the octahedra are occupied by hydroxyl groups to generate −Al−O− chains connected by 2 to form a 3D framework with the empirical formula Al(OH)(2)-(DMF)₁.₈(H₂O)₃.₅. Analogues of these MOFs were synthesized from ligand 1. UiO-67-dcppy and DUT-5-dcppy were synthesized by combining ZrCl₄ or AlCl₃·6H₂O with 1 in DMF. UiO-67-dcppy and DUT-5-dcppy were shown to possess the same structures as the parent UiO-67 and DUT-5 frameworks as evidenced by PXRD analysis (Figure 1). ¹H
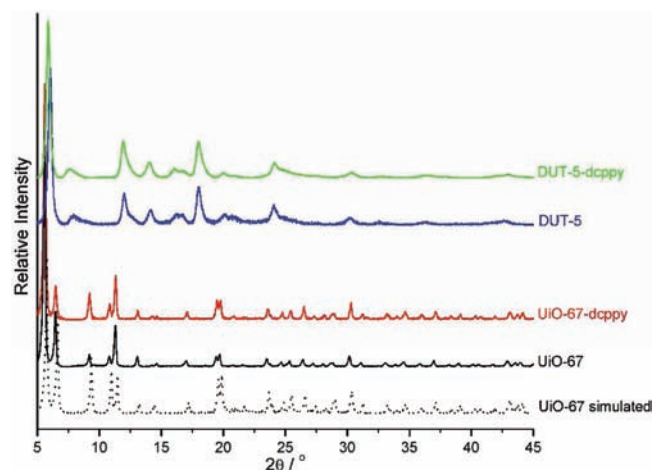

Figure 1. PXRD patterns of UiO-67, UiO-67-dcppy, DUT-5, and DUT-5-dcppy.

NMR analysis of digested samples of these frameworks showed that ligand 1 remained intact under the solvothermal synthesis conditions. UiO-67-dcppy and DUT-5-dcppy were found to have thermostability up to ~550 °C, which is comparable to their parent frameworks.

Upon finding that UiO-67-dcppy and DUT-5-dcppy could be readily prepared, the compatibility of 1 with different types of MOFs was examined by introducing the ligand into three-dimensional (3D) pillared Zn-paddlewheel MOFs. These pillared, mixed-ligand frameworks have been widely studied and some have been shown to display framework flexibility.[32−36] The dimensions of these mixed-ligand MOFs can be adjusted independently in two dimensions by replacing either (or both) the bridging dicarboxylate and pillaring dinitrogen ligands. Ligands 1 or 2 were combined with dabco and Zn(NO₃)₂·6H₂O in DMF to afford DMOF-1-dcppy and DMOF-1-bpdc (DMOF = dabco MOF), respectively. PXRD and single X-ray diffraction analysis of DMOF-1-dcppy and DMOF-1-bpdc revealed that these two MOFs possess the same framework topology (Figure 3). These materials are structural analogues of the DMOF framework previously reported by Kim and co-workers.[37] These structures contain Zn²⁺-paddlewheel

SBUs, connected together by the carboxylate ligands into 2D sheets. These 2D sheets are linked by pillaring dabco ligands that coordinate to the axial sites on the SBUs giving 3D frameworks of $Zn_2(L)_2(dabco)$ (where L = **1** or **2**). Both frameworks contained large rectangular and square (type-α)[38] channels along the crystallographic *b*-axis and *c*-axis, respectively (channel diameters of approximately 21.5 Å and 18 Å, Figure 2).
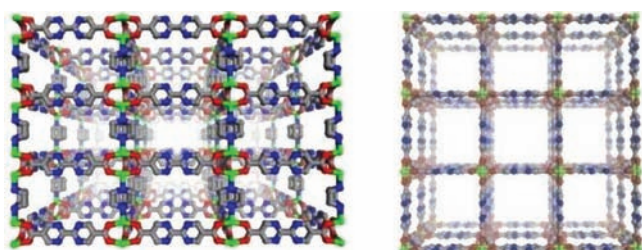

Figure 2. Ball and stick perspective views along the crystallographic *b*-axis (left) and *c*-axis (right) of DMOF-1-dcppy framework. The DMOF-1-bpdc framework is isostructural. Note that the nitrogen atom of ligand **1** is shown disordered over four possible positions. Color scheme: carbon (gray), nitrogen (blue), oxygen (red), and zinc (green).

The ability to enlarge the size of frameworks to obtain pore-expanded, isoreticular analogues is a central tenet in the development of MOFs.[39] Thus, in an attempt to extend the dimensions of DMOF-1-dcppy and DMOF-1-bpdc, the dabco ligand was replaced with 4,4′-bipyridine (4,4′-bpy), a longer pillaring linker. BMOF-1-dcppy and BMOF-1-bpdc (BMOF = 4,4′-bipyridine MOF) were obtained by combining **1** or **2** with 4,4′-bpy and $Zn(NO_3)_2 \cdot 6H_2O$ in DMF. Characterization of BMOF-1-dcppy and BMOF-1-bpdc by single-crystal X-ray diffraction showed that both compounds possess the expected paddlewheel SBU and overall 3D net topology as found for the DMOF frameworks.[37] However, these 3D nets possess distorted rectangular and rhomboid (type-β)[38] channels along the crystallographic *b*-axis and *c*-axis. While the channels of BMOF-1-dcppy display a rhomboid distortion, the channels of BMOF-1-bpdc are only slightly distorted from a perfect square (Figure 3). The PXRD results of BMOF-1-dcppy and BMOF-1-bpdc revealed some differences in reflections at $2\theta > 7°$ (Figure 4). Similar observations have also been reported for interpenetrated Zn-paddlewheel DUT-8 due to the flexibility of the framework.[40] In addition, the pores of BMOF-1-dcppy and BMOF-1-bpdc are big enough to accommodate a second
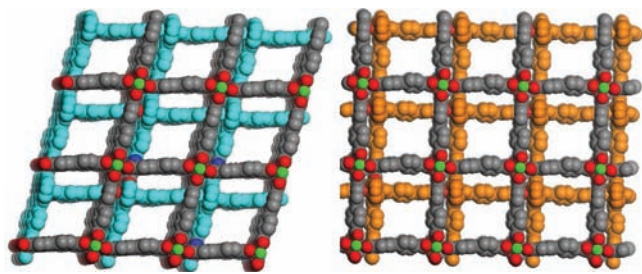

Figure 3. Space-filling views along the crystallographic *c*-axis of BMOF-1-dcppy (left) and BMOF-1-bpdc (right). In each image one framework is shown colored by atom and the interpenetrated framework is shown as a single, solid color. Color scheme: carbon (gray), nitrogen (blue), oxygen (red), and zinc (green).
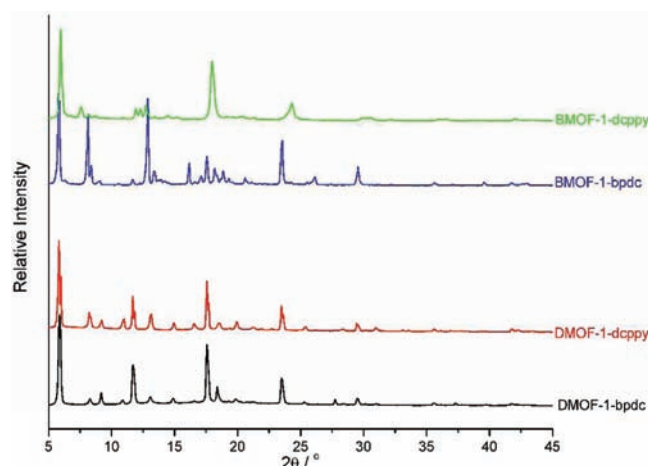

Figure 4. PXRD of DMOF-1-bpdc, DMOF-1-dcppy, BMOF-1-bpdc, and BMOF-1-dcppy.

interpenetrating framework, giving an overall 2-fold inter-penetrated structure. Because of interpenetration, there are two different channels along the *c*-axis, but only one channel along the *b*-axis.

Gas sorption experiments were performed to evaluate the porosity of these new MOFs. The rigid UiO-67-dcppy was found to have a BET surface area of 1535 ± 324 m²/g, which is comparable to that found for UiO-67 (1615 ± 345 m²/g). Similarly, the BET surface area of DUT-5-dcppy was found to be 827 ± 38 m²/g, which is similar to the parent DUT-5 (711 ± 129 m²/g).

In contrast to the rigid UiO and DUT frameworks, DMOF-1-dcppy and DMOF-1-bpdc gave low BET surface areas of 118 ± 12 m²/g and 185 ± 31 m²/g, respectively. Even at ambient pressures ($P/P_o = 1$), DMOF-1-dcppy and DMOF-1-bpdc show low N_2 uptake at 77 K (<50 cm³/g), much lower than DMOF-1 (BET surface area =1450 m²/g),[37] which is an unexpected result based on the size of the channels found crystallographically (Figure 5). The low uptake of N_2 prompted the examination of these frameworks with CO_2 at 196 K (Figure 6). Similar to N_2 uptake, uptake of CO_2 in DMOF-1-dcppy and DMOF-1-bpdc remains low up to 760 mmHg (<100 cm³/g). The PXRD patterns of the activated DMOF-1-dcppy and DMOF-1-bpdc showed differences in the reflections at
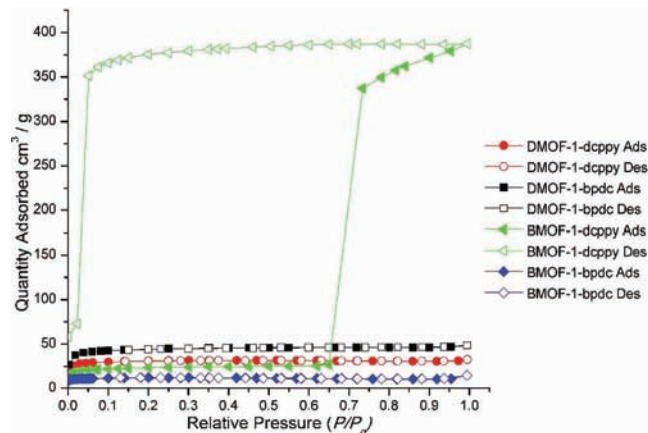

Figure 5. N_2 isotherm of DMOF-1-bpdc, DMOF-1-dcppy, BMOF-1-bpdc, and BMOF-1-dcppy at 77 K.

high-angles, as well as peak-broadening (Figure S15, Supporting Information). These differences may be due to a phase-transition of framework or to degradation of the framework upon activation. It is not uncommon that the DMOF framework shows peak broadening in the PXRD upon activation. However, the changes in the positions of specific reflections are generally indicative of a phase-transition of the framework.[41−44] For example, in a series of bifunctional DMOF materials, a group of porous (DMOF-2,3-NH$_2$X, X = halide) and nonporous (DMOF-2,5-NH$_2$X) derivatives were identified. The PXRD patterns of both activated DMOFs show peak broadening, but only nonporous DMOF-2,5-NH$_2$X shows the change in the position of low-angle reflections.[44] On the basis of these previous studies, we cannot completely rule out degradation of DMOF-1-dcppy and DMOF-1-bpdc as a source of the low surface areas, but the shift in the low-angle reflections is consistent with a phase-transition of the frameworks to a narrow-pore type isomorph.

Even more distinct from the MOFs described above was the gas sorption behavior of BMOF-1-dcppy. BMOF-1-dcppy showed distinct behavior in N$_2$ and CO$_2$ uptake when compared to the other MOFs prepared here, including DMOF-1-dcppy and DMOF-1-bpdc. The N$_2$ adsorption isotherm at 77 K for BMOF-1-bpdc shows a low uptake capacity. Similarly, BMOF-1-dcppy shows low N$_2$ uptake from P/P_o = 0 − 0.74. However, above $P/P_o \approx 0.74$ a large increase in gas sorption is observed, resulting in a final uptake of ∼386 ± 12 cm^3/g at $P/P_o \sim 1$ (Figure 5). The dramatic change in gas sorption behavior indicates the framework undergoes a phase change, potentially from a narrow pore to a large pore form.[6] Interestingly, desorption of N$_2$ showed a pronounced hysteresis, with essentially no release of the gas until P/P_o < 0.05. The CO$_2$ adsorption isotherm at 196 K of BMOF-1-dcppy and BMOF-1-bpdc showed similar behavior as that observed with N$_2$ (Figure 6). While BMOF-1-bpdc uptakes a
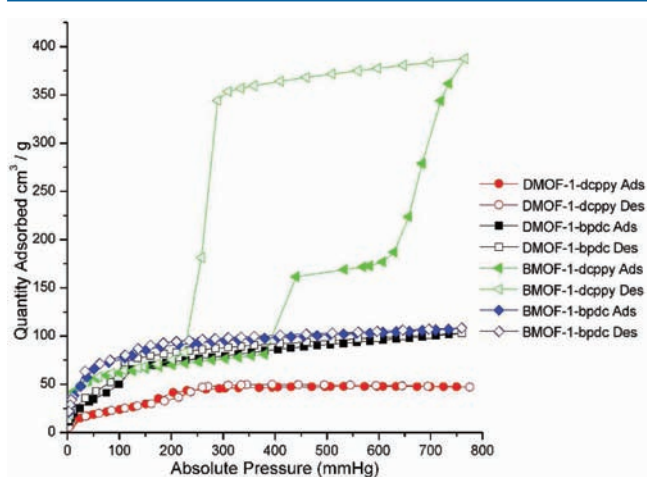

Figure 6. CO$_2$ isotherms of DMOF-1-bpdc, DMOF-1-dcppy, BMOF-1-bpdc, and BMOF-1-dcppy at 196 K.

moderate amount of CO$_2$ (∼21 wt % at 760 mmHg) without any hysteresis, BMOF-1-dcppy exhibited a higher CO$_2$ capacity with a notable hysteresis. At low pressure (0−380 mmHg), BMOF-1-dcppy showed low CO$_2$ uptake, but above 380 mmHg, an increased uptake was observed, indicative of a phase-transition, potentially from a closed-form to a "semi-open" form. At even higher pressures (630 mmHg), BMOF-1-

dcppy showed another step in the sorption isotherm, indicating a second phase-transition, presumably from the *semi*-open to the open form. Overall, the framework showed a high uptake of CO$_2$ at 196 K (75 wt % at 760 mmHg). In addition, the desorption isotherm displayed only one phase-transition at 300 mmHg that appears to be directly to the closed-pore form.

The PXRD patterns of the activated BMOF-1-dcppy and BMOF-1-bpdc show substantial differences when compared to the as-synthesized MOFs. Unlike the activated DMOF-1-dcppy and DMOF-1-bpdc, the PXRD patterns of activated BMOFs show much less peak broadening, indicative of better crystallinity upon activation (Figure S16, Supporting Information). Cell refinement was performed on the PXRD patterns of the activated BMOFs, which showed shrinkage in cell dimensions and volume (Table S2, Supporting Information). This observation was supported by the low gas uptake capacity of these MOFs at low pressure. However, the gas sorption behavior of BMOF-1-dcppy is different from BMOF-1-bpdc at higher pressure ($P/P_o \approx 0.74$). As BMOF-1-dcppy and BMOF-1-bpdc are virtually identical materials, the differences in gas sorption behavior between the MOFs can be best attributed to the pyridine ring in ligand **1**. On the basis of crystallographic data (Figure 3), the major interaction between the two interpenetrated nets in both solvated MOFs comes from a $\pi-\pi$ interaction between the ligands (Figure 7). Specifically,
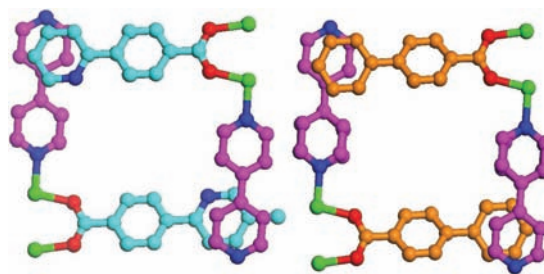

Figure 7. Interactions between the interpenetrated frameworks in BMOF-1-dcppy (left) and BMOF-1-bpdc (right). The disorder of the nitrogen atom of **1** (dcppy) has been removed for clarity. Color scheme: nitrogen (blue), oxygen (red), and zinc (green), 4,4'-bpy (pink), **1** (dcppy, cyan), and **2** (bpdc, orange).

the closest points of contact are between the carboxylate ligands (**1** or **2**) and the pillaring ligand (4,4'-bpy). While BMOF-1-dcppy presents the equivalent of a "pyridine dimer" interaction, BMOF-1-bpdc exhibits a "benzene-pyridine" dimer (Figure 7). In both case, the rings are stacked in parallel-displaced configuration as determined from the X-ray diffraction data.[45,46] Computational studies have indicated that benzene−pyridine dimers generally have stronger interactions when compared to those of pyridine dimers. Only when the nitrogen atoms of each rings are 180° opposed from each other is the interaction in a pyridine−pyridine dimer stronger; however, this configuration is not accessible in the MOFs. Because of the weaker $\pi-\pi$ interactions between the frameworks in BMOF-1-dcppy, it should be easier for guest molecules to disrupt the interframework interactions when compared to BMOF-1-bpdc. Disruption of the interframework (pyridine dimer) interactions might be what allows for BMOF-1-dcppy to undergo phase-transition, potentially from a closed- to open-pore structure at higher gas pressures. This hypothesis assumes that some variation of these $\pi-\pi$ interactions is maintained in these interpenetrated MOFs upon activation.

Regardless of the specific origin of these phenomena, these experiments demonstrate that even single-atom changes to the ligands in a MOF can result in substantial differences in physical properties such as gas sorption and framework structural transitions.

■ CONCLUSIONS

In conclusion, we have presented the integration of a pyridine-phenyl ligand into several different MOFs. More importantly, the pyridine nature of **1** is found to produce a significant effect on the gas sorption behavior of the interpenetrated BMOF-1-dcppy. The observed phase transition is attributed to weak interframework interactions, which are strengthened in the case of BMOF-1-bpdc, which does not display hysteresis. Future efforts will focus on the rich cyclometalation chemistry of ligand **1** and its use in preparing functionalized MOFs.

■ ASSOCIATED CONTENT

ⓢ Supporting Information

Detailed synthesis and characterization of ligand, MOFs characterization, and cif files This material is available free of charge via the Internet at http://pubs.acs.org.

■ AUTHOR INFORMATION

Corresponding Author

*E-mail: scohen@ucsd.edu.

Notes

The authors declare no competing financial interest.

■ ACKNOWLEDGMENTS

■ REFERENCES

(1) Murray, L. J.; Dinca, M.; Long, J. R. *Chem. Soc. Rev.* **2009**, *38*, 1294.
(2) Li, J.-R.; Kuppler, R. J.; Zhou, H.-C. *Chem. Soc. Rev.* **2009**, *38*, 1477.
(3) Lee, J.; Farha, O. K.; Roberts, J.; Scheidt, K. A.; Nguyen, S. T.; Hupp, J. T. *Chem. Soc. Rev.* **2009**, *38*, 1450.
(4) McKinlay, A. C.; Morris, R. E.; Horcajada, P.; Ferey, G.; Gref, R.; Couvreur, P.; Serre, C. *Angew. Chem., Int. Ed.* **2010**, *49*, 6260.
(5) Kitagawa, S.; Kondo, M. *Bull. Chem. Soc. Jpn.* **1998**, *71*, 1739.
(6) Ferey, G.; Serre, C. *Chem. Soc. Rev.* **2009**, *38*, 1380.
(7) Kitagawa, S.; Uemura, K. *Chem. Soc. Rev.* **2005**, *34*, 109.
(8) Salles, F.; Maurin, G.; Serre, C.; Llewellyn, P. L.; Knofel, C.; Choi, H. J.; Filinchuk, Y.; Oliviero, L.; Vimont, A.; Long, J. R.; Ferey, G. *J. Am. Chem. Soc.* **2010**, *132*, 13872.
(9) Wang, Z.; Cohen, S. M. *J. Am. Chem. Soc.* **2009**, *131*, 16675.
(10) Chun, H.; Dybtsev, D. N.; Kim, H.; Kim, K. *Chem.—Eur. J.* **2005**, *11*, 3521.
(11) Hocarjada, P.; Salles, F.; Wuttke, S.; Devic, T.; Heurtaux, D.; Maurin, G.; Vimont, A.; Daturi, M.; David, O.; Magnier, E.; Stock, N.; Filinchuk, Y.; Popov, D.; Riekel, C.; Ferey, G.; Serre, C. *J. Am. Chem. Soc.* **2011**, *133*, 17839.
(12) Maji, T. K.; Matsuda, R.; Kitagawa, S. *Nat. Mater.* **2007**, *6*, 142.

(13) Henke, S.; Florian Wieland, D. C.; Meilikhov, M.; Paulus, M.; Sternemann, C.; Yusenko, K.; Fischer, R. A. *CrystEngComm* **2011**, *13*, 6399.
(14) Kim, J.; Chen, B.; Reineke, T. M.; Li, H.; Eddaoudi, M.; Moler, D. B.; O'Keeffe, M.; Yaghi, O. M. *J. Am. Chem. Soc.* **2001**, *123*, 8239.
(15) Ferey, G. *Chem. Soc. Rev.* **2009**, *37*, 191.
(16) Kitagawa, S.; Kitaura, R.; Noro, S.-I. *Angew. Chem., Int. Ed.* **2004**, *43*, 2334.
(17) Yaghi, O. M.; O'Keeffe, M.; Ockwig, N. W.; Chae, H. K.; Eddaoudi, M.; Kim, J. *Nature* **2003**, *423*, 705.
(18) Rowsell, J. L. C.; Yaghi, O. M. *Microporous Mesoporous Mater.* **2004**, *73*, 3.
(19) Deng, H.; Doonan, C. J.; Furukawa, H.; Ferreira, R. B.; Towne, J.; Knobler, C. B.; Wang, B.; Yaghi, O. M. *Science* **2010**, *327*, 846.
(20) Gust, D.; Moore, T. A.; Moore, A. L. *Acc. Chem. Res.* **2009**, *42*, 1890.
(21) Concepcion, J. J.; Jurss, J. W.; Brennaman, M. K.; Hoertz, P. G.; Patrocinio, A. O. v. T.; Murakami Iha, N. Y.; Templeton, J. L.; Meyer, T. J. *Acc. Chem. Res.* **2009**, *42*, 1954.
(22) Esswein, M. J.; Nocera, D. G. *Chem. Rev.* **2007**, *107*, 4022.
(23) Dubois, M. R.; Dubois, D. L. *Acc. Chem. Res.* **2009**, *42*, 1974.
(24) Morris, A. J.; Meyer, G. J.; Fujita, E. *Acc. Chem. Res.* **2009**, *42*, 1983.
(25) Lyons, T. W.; Sanford, M. S. *Chem. Rev.* **2010**, *110*, 1147.
(26) Bloch, E. D.; Britt, D.; Lee, C.; Doonan, C. J.; Uribe-Romo, F. J.; Furukawa, H.; Long, J. R.; Yaghi, O. M. *J. Am. Chem. Soc.* **2008**, *132*, 14382.
(27) Wang, C.; Xie, Z.; deKrafft, K. E.; Lin, W. *J. Am. Chem. Soc.* **2011**, *133*, 13445.
(28) Cavka, J. H.; Jakobsen, S.; Olsbye, U.; Guillou, N.; Lamberti, C.; Bordiga, S.; Lillerud, K. P. *J. Am. Chem. Soc.* **2008**, *130*, 13850.
(29) Senkovska, I.; Hoffmann, F.; Froba, M.; Getzschmann, J.; Bohlmann, W.; Kaskel, S. *Microporous Mesoporous Mater.* **2009**, *122*, 93.
(30) Sheldrick, G. M. *Acta Crystallogr.* **2008**, *A64*, 112.
(31) Spek, A. L. *Acta Crystallogr.* **2009**, *D65*, 148.
(32) Chun, H.; Dybtsev, D. N.; Kim, H.; Kim, K. *Chem.—Eur. J.* **2005**, 3521.
(33) Kitaura, R.; Seki, K.; Akiyama, G.; Kitagawa, S. *Angew. Chem., Int. Ed.* **2005**, *42*, 428.
(34) Ma, B.-Q.; Mulfort, K. L.; Hupp, J. T. *Inorg. Chem.* **2005**, *44*, 4912.
(35) He, H.; Yuan, D.; Ma, H.; Sun, D.; Zhang, G.; Zhou, H.-C. *Inorg. Chem.* **2010**, *49*, 7605.
(36) Mulfort, K. L.; Farha, O. K.; Malliakas, C. D.; Kanatzidis, M. G.; Hupp, J. T. *Chem.—Eur. J.* **2010**, *16*, 276.
(37) Dybtsev, D. N.; Chun, H.; Kim, K. *Angew. Chem., Int. Ed.* **2004**, *43*, 5033.
(38) Uemura, K.; Yamasaki, Y.; Onishi, F.; Kita, H.; Ebihara, M. *Inorg. Chem.* **2010**, *49*, 10133.
(39) Furukawa, H.; Ko, N.; Go, Y. B.; Aratani, N.; Choi, S. B.; Choi, E.; Yazaydin, A. O.; Snurr, R. Q.; O'Keeffe, M.; Kim, J.; Yaghi, O. M. *Science* **2010**, *239*, 424.
(40) Hauptvogel, I. M.; Biedermann, R.; Klein, N.; Senkovska, I.; Cadiau, A.; Wallacher, D.; Feyerherm, R.; Kaskel, S. *Inorg. Chem.* **2011**, *50*, 8367.
(41) Kim, M.; Boissonnault, J. A.; Dau, P. V.; Cohen, S. M. *Angew. Chem., Int. Ed.* **2011**, *50*, 12193.
(42) Ghosh, S. K.; Zhang, J.-P.; Kitagawa, S. *Angew. Chem., Int. Ed.* **2007**, *46*, 7965.
(43) Chen, B.; Ma, S.; Zapata, F.; Fronczek, F. R.; Lobkovsky, E. B.; Zhou, H.-C. *Inorg. Chem.* **2007**, *46*, 1233.
(44) Comotti, A.; Bracco, S.; Sozzani, P.; Horike, S.; Matsuda, R.; Chen, J.; Takata, M.; Kubota, Y.; Kitagawa, S. *J. Am. Chem. Soc.* **2008**, *130*, 13664.
(45) Hohenstein, E. G.; Sherrill, C. D. *J. Phys. Chem. A* **2009**, *113*, 878.
(46) Smith, Q. A.; Gordon, M. S. *J. Phys. Chem. A* **2011**, *115*, 4598.